RADIATION-PRESSURE ENHANCED OPTO-ACOUSTIC OSCILLATOR

Matthew J. Storey, Siddharth Tallur, and Sunil A. Bhave
Cornell University, Ithaca, USA

ABSTRACT

This paper presents a driving scheme for silicon opto-acoustic oscillators (OAO) by simultaneously exploiting radiation-pressure (RP) and RF feedback oscillation mechanisms to achieve significantly lower phase noise than could be realized by either phenomenon solely. A theoretical model and experimental results are presented corroborating this scheme, demonstrating a silicon OAO operating at 175 MHz with a phase noise of -128.6 dBc/Hz at 1 MHz offset with 2.77 dBm RF output power, resulting in a 10dB far-from-carrier phase noise improvement.

INTRODUCTION

Reference oscillators are ubiquitous elements used in virtually every communication system in existence. The need for miniaturized, batch manufacturable oscillators as chip scale timing references stems from the need to replace the well-established, high performing, albeit expensive quartz oscillators without compromising on performance. MEMS oscillators have recently found applications in various consumer electronic applications. With numerous advances in fabrication technology and materials processing, these oscillators are being pushed to create a presence in the high performance base-band market and high frequency applications. Scaling MEMS oscillators to high frequencies presents challenges in terms of reduced transduction efficiencies and material limits on quality factors. Opto-mechanical transduction offers higher sensitivity and opens up possibilities to interrogate high frequency mechanical resonances hitherto inaccessible. In the past, our group has demonstrated an opto-mechanically transduced MEMS oscillator designed in silicon nitride with zero flicker noise [1], which greatly simplifies the oscillator design and does away with active noise sources that would otherwise add flicker noise, thereby degrading the oscillator phase noise.

Opto-mechanical resonator based oscillators have been previously demonstrated in both open and closed loop configurations utilizing radiation–pressure (RP) [1,2] and RF feedback (RF) [3], respectively. Simultaneous incorporation of these oscillating mechanisms can be achieved with a 2-coupled-ring opto-mechanical resonator. Figure 1 shows an SEM of our device. The coupled resonator can be transduced through either capacitive electrostatics or evanescent optical coupling. While each ring utilizes a different forcing mechanism, the displacement is conserved and transferred between ring resonators through the λ/2 coupling beam.

In the following sections, a model is presented for the 2-coupled-ring opto-mechanical cavity dynamics utilizing both RP and RF feedback forces. This model was non-dimensionalized to examine the relative affects between
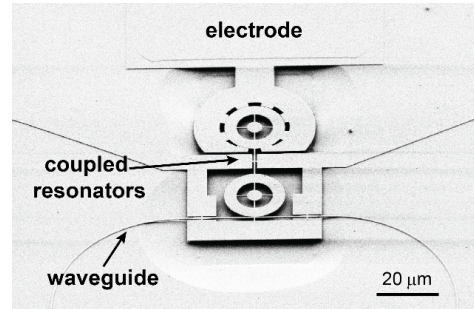

Figure 1: Scanning electron micrograph (SEM) of the 2-coupled-ring resonator. The resonator-waveguide gap is 100nm, each ring has an inner radius of 5.7µm and outer radius of 9.5µm and the resonator-electrode gap is 130nm.

these driving mechanisms and simulations were performed. The 2-coupled-ring resonator was fabricated and tested in vacuum at low temperatures under three operating conditions - RP, RF feedback, and both simultaneously. The phase noise of the oscillator was measured in all three cases and compared at both close-to-carrier and far-from-carrier offset frequencies. We present and discuss these results in subsequent sections.

OAO MODEL
Theoretical Framework

The dynamics of an opto-mechanical cavity have been extensively studied in previous work [4]. The displacement u and optical field $\sqrt{\hbar\Omega_L}a$ inside the cavity are related through the following coupled equations of motion [5]

$$m\ddot{u} + m\gamma_0\dot{u} + m\Omega_0{}^2 u = F_{rp} + F_{rf}, \qquad (1)$$

$$\dot{a} = i(\Delta_0 + g_{om}u)a - \tfrac{1}{2}\kappa a + \tfrac{1}{2}\kappa n_{max}^{1/2}. \qquad (2)$$

Here, Ω_0 is the mechanical resonance frequency, m is the effective mass, and γ_0 is natural damping of the harmonic resonator. The total optical cavity detuning $\Delta = \Delta_0 + g_{om}u$ is a function of both the laser detuning at zero displacement Δ_0, the dynamic displacement of the cavity u, and the opto-mechanical coupling coefficient g_{om}. The total (loaded) optical linewidth $\kappa = \kappa_i + \kappa_{ex}$ can be expressed as a sum of the intrinsic and extrinsic (coupling) linewidths, respectively. The normalized intra cavity photon number can be expressed as $n = |a|^2$ and the input power P_{in} can be expressed in terms of the maximum intra cavity photon number $n_{max} = 4P_{in}\kappa_{ex}/\kappa^2\hbar\Omega_L$ [5].

The 2-coupled-ring design of our opto-mechanical resonator allows for a unique transduction scheme via simultaneous forcing through both radiation pressure and

capacitive electrostatic forces. The force on the cavity generated through radiation pressure is only dependent on the opto-mechanical coupling coefficient and the intra cavity photon number $F_{rp} = \hbar g_{om} n$ [5].

The RF electrostatic force, however, depends on the feedback loop design incorporating the resonator. In our setup, the cavity's output optical power is sent to a photodetector and converted into a photocurrent. The optical field transmitted from the cavity can be expressed in terms of the input optical field and intra cavity field $a_{out} = a_{in} - \sqrt{\kappa_{ex}}a$ where $|a_{out}|^2$ is normalized to the output power and $|a_{in}|^2$ is normalized to the input power (P_{in}) [6]. The total photocurrent is proportional to the output power

$$i_{tot} = |a_{out}|^2 = |a_{in}|^2 + \kappa_{ex}n - 2\,Re\{a_{in}^* a\sqrt{\kappa_{ex}}\}. \quad (3)$$

Since the input power is constant, the current fluctuations are contained in the difference between the output and input power. Therefore, the photocurrent that is fed back to the resonator can be expressed as $i_{rf} = |a_{out}|^2 - |a_{in}|^2$. The photocurrent is then amplified (gain G) with appropriate phase shift and electrostatically applied to the opto-mechanical resonator to close the feedback loop. The general forcing function for the RF feedback is given as $F_{rf} = G i_{rf}$ [7].

Non-dimensionalized Dynamics

To better understand the relative interaction between these two forcing mechanisms, the coupled equations of motion are put into a dimensionless form [5]

$$\tilde{u}'' + \tilde{\gamma}_0 \tilde{u}' + \tilde{u} = c_{om}\tilde{n} + c_{om}\tilde{G}\big(\tilde{\kappa}_{ex}\tilde{n} - 2\sqrt{\tilde{\kappa}_{ex}}Re\{\tilde{a}\}\big), \quad (4)$$

$$\tilde{a}' = i\big(\tilde{\Delta}_0 + \tilde{u}\big)\tilde{a} - \tfrac{1}{2}\tilde{\kappa}\tilde{a} + \tfrac{1}{2}\tilde{\kappa}. \quad (5)$$

Here, the time was scaled by the mechanical resonance frequency $\tau = \Omega_0 t$ and the displacement was scaled as $\tilde{u} = u\,g_{om}/\Omega_0$. All other frequencies were scaled by Ω_0 [5] such that $\tilde{\gamma}_0 = \gamma_0/\Omega_0$, $\tilde{\kappa} = \kappa/\Omega_0$, and $\tilde{\Delta}_0 = \Delta_0/\Omega_0$. The normalized extrinsic linewidth is a fraction of the total normalized linewidth, which depends on the coupling. In general, $\tilde{\kappa}_{ex} = \mu\tilde{\kappa}$ where $0 < \mu < 1$, but for the rest of this analysis the device is assumed to be critically coupled such that $\mu = 0.5$.

The intra cavity optical field was normalized by the maximum photon number such that $\tilde{a} = a/\sqrt{n_{max}}$ and $\tilde{n} = n/n_{max}$. The strength of the radiation pressure force was scaled as $c_{om} = 2n_{max}u_{zpm}^2 g_{om}^2/\Omega_0^2$ and a detailed explanation of the radiation pressure coupling strength can be found in [5]. The strength of the RF feedback force is both a combination of the input optical power contained in c_{om} and the scaled gain $\tilde{G}$ from the amplifier. Therefore, the total dimensionless strength of the closed loop RF feedback force is given by $c_{om}\tilde{G}$.

Phase Noise Improvement

Assuming the harmonic oscillations of the opto-mechanical cavity have an energy that is proportional to the square of the displacement, the oscillation linewidth can be expressed as [8]

$$\delta v = \Delta v \left(\frac{k_B T}{m_{eff}\Omega_0^2}\right)\frac{1}{u^2}. \quad (6)$$

Here, δv is the narrowed linewidth, Δv is the natural linewidth of the resonator, and m_{eff} is the effective mass. The relationship between the oscillator's linewidth and its phase noise $\mathcal{L}$ (dBc/Hz) at a carrier offset frequency Δf in the $1/f^2$ regime is given by [8]

$$\delta v = 2\pi\Delta f^2 10^{\mathcal{L}/10}. \quad (7)$$

By only varying the driving schemes of an OAO, a change in the displacement can vary the degree in which the linewidth narrows. This in turn can change the phase noise at a given carrier offset. Equations (6) and (7) were combined and the phase noise difference at a constant offset was solved for as a function of the displacement ratio

$$\Delta\mathcal{L} = \mathcal{L}_2 - \mathcal{L}_1 = 20\,log_{10}\big(u_1/u_2\big). \quad (8)$$

The equation above shows that the phase noise improvement is proportional to the ratio of oscillation energies. Therefore, if the displacement of second driving scheme is larger than the first driving scheme ($u_2 > u_1$), then there will be an improvement in the phase noise ($\Delta\mathcal{L} < 0$).

Numerical Simulations

The relative displacements of the different driving schemes were compared by numerically integrating equations (4) and (5) for different cases of c_{om} and $\tilde{G}$. Our OAO operates in the unresolved sideband regime (USR) and typically exhibit mechanical quality factors on the order of a couple thousand, so the dimensionless parameters chosen were $\tilde{\gamma}_0 = 0.0005$, $\tilde{\kappa} = 10$, and $\tilde{\Delta}_0 = 3$ [5].

The values for c_{om} and $\tilde{G}$ for the three cases are determined from the threshold behavior of both the RF feedback and radiation pressure induced oscillations. The threshold for radiation pressure oscillations was found to be $c_{om} \approx 0.015$ and the threshold for closed loop RF feedback was $c_{om}\tilde{G} \approx 0.007$.

The first case is just RP oscillations, so the amplifier gain was set to $\tilde{G} = 0$ and the radiation pressure coupling coefficient was set to twice the threshold at $c_{om} = 0.03$. The second case is for just RF feedback, so the radiation pressure force is set well below threshold at $c_{om} = 0.005$ and the amplifier gain was set to just above RF feedback threshold at $\tilde{G} = 2$. In the third case, both forces were placed above threshold. Since the RF feedback force is a function of both gain terms, two comparisons arise for RP enhanced RF feedback oscillations. As c_{om} is raised above
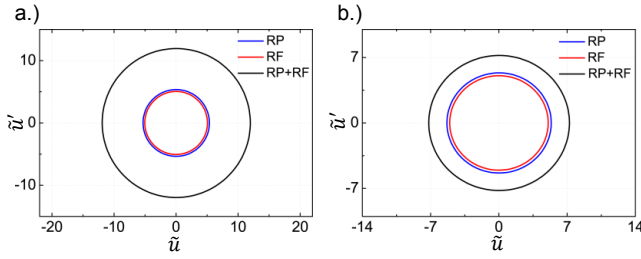
Figure 2: Limit cycle comparisons of the three driving schemes. For RP enhanced RF feedback, plot (a) is when amplifier gain is held constant and plot (b) is for the total closed loop gain held constant.

threshold (0.03), either the amplifier gain $\tilde{G}$ can be held constant at 2 or the total closed loop gain can be held constant at $c_{om}\tilde{G} = 0.01$, which requires reducing the amplifier gain to $\tilde{G} = 1/3$.

Figure 2 shows the simulation results of the three cases. When the driving scheme was only radiation pressure or RF feedback, the oscillator reached a steady limit cycle with scaled displacement amplitude of approximately 5. When both driving schemes were incorporated while holding the amplifier gain constant, the scaled amplitude reached a value of 12 (plot (a) of figure 2). If the total closed loop gain was held constant, the scaled amplitude reached a value of 7.2 (plot (b) of figure 2). Plugging these values into equation (8), the resulting phase noise improvement would be approximately 8 dB and 3 dB, respectively.

EXPERIMENTAL SETUP

The 2-coupled-ring opto-mechanical resonator was fabricated on a silicon-on-insulator (SOI) wafer and the fabrication process was described in detail in [3]. All experiments were performed in a Lakeshore probe station under vacuum (30μTorr) using Liquid Nitrogen to cool the chamber to 80 K. An optical probe was used to send continuous wave (CW) light into the device through a pair of on-chip grating couplers. A GSG probe was used to apply an RF signal to the bond pads, which connected to the
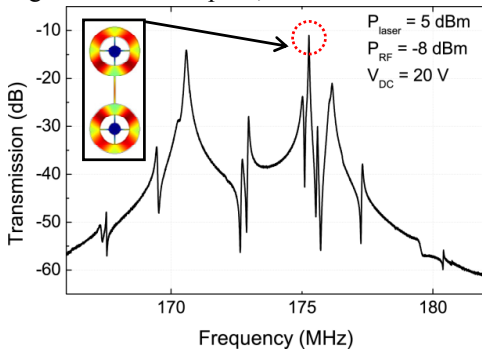

Figure 3: RF Transmission spectrum for the opto-acoustic resonator measured in vacuum (30μTorr) and low temperature (80 K). The mechanical mode at 175.3 MHz corresponds to the fundamental radial expansion mode (inset: mode-shape) with a quality factor of 6,000.
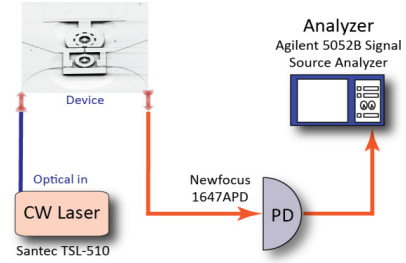

Figure 4: Experimental setup for radiation pressure oscillations

electrodes around the resonator.

Open loop measurements were performed on the opto-acoustic resonator to determine the RF transmission spectrum of the mechanical mode of interest. As the applied RF signal was swept, the transmitted power was sent to a photodetector and the resulting photocurrent was input to a Network Analyzer. Figure 3 shows the electromechanical transmission measurement for the fundamental radial mode. The resonance frequency (175.3 MHz) and mechanical quality factor (6,000) were estimated through a Lorentzian curve fit.

For comparison purposes, the phase noise performance of the opto-mechanical resonator based oscillator was first evaluated for RP and RF feedback separately. Since the RP and RF feedback driving mechanisms differ in their application to the resonator, this experiment required two separate setups. Figure 4 shows the setup for a RP driven opto-mechanical oscillator. A CW diode laser was input to the device and then the output optical power is measured with a Newfocus 1647 photodetector and sent to the phase noise analyzer. RP induced oscillations are achieved by blue detuning the laser within the optical resonance and using an input power above threshold [1,2].

To ensure that the only means of achieving oscillations is by closing the feedback loop, the laser power is reduced below the threshold for RP oscillations. To create a RF feedback oscillator, the output RF signal from the photodetector is amplified and the required phase shift is introduced to overcome the FB oscillation threshold. The signal is sent through a 3dB splitter and one half is applied to the resonator through the GSG probe while the other half
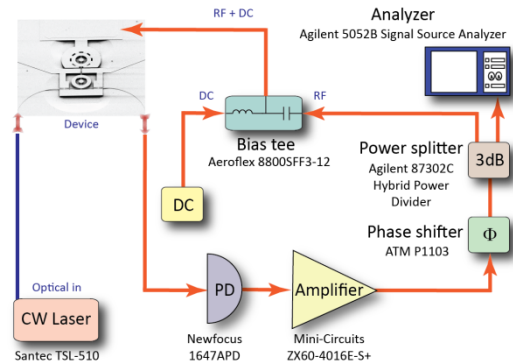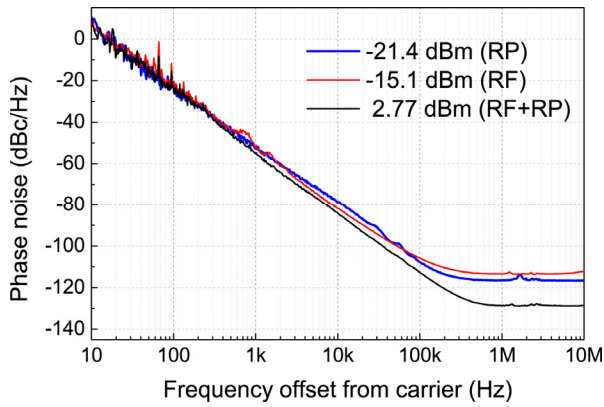

Figure 5: Experimental setup for feedback oscillations

Figure 6: Phase noise data for all three driving mechanisms. For each plot, the RF output signal power and driving scheme is given.

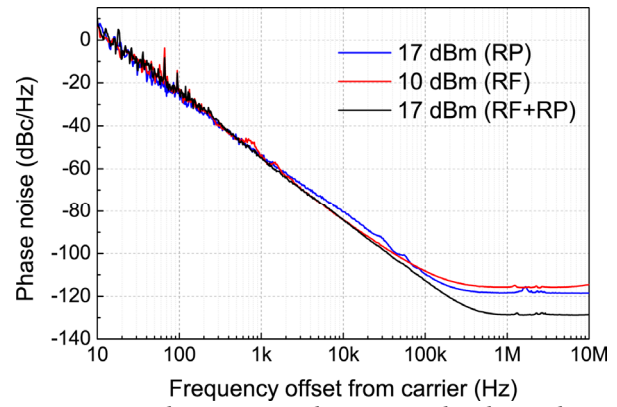*Figure 7: Phase noise data normalized to the power consumption. For each plot, the input optical power and driving scheme is given.*

is sent to the phase noise analyzer. Figure 5 shows the experimental setup for the RF feedback oscillator. To achieve oscillations induced simultaneously by both RP and RF feedback, the closed loop setup shown in Figure 5 is used with the laser blue detuned and with the optical power raised above RP threshold conditions.

RESULTS

Using the setup in figure 4, the device was driven into RP oscillations at an input optical power of 17 dBm with a determined RP threshold of 11 dBm. The setup in figure 5 was then used to obtain RF feedback oscillations with an input optical power below RP threshold (10 dBm). While in the same closed loop configuration, the input optical power was increased well above threshold (17 dBm) to observe RP enhanced RF feedback oscillations. Any further increase in laser power would result in thermal nonlinearities and chaotic oscillations. All of the closed loop measurements were carried out with 30 V DC bias. Figure 6 shows the resulting phase noise for the three measurements, along with the carrier powers and driving scheme. The individual RP and RF feedback oscillations had the lowest carrier powers (-21.4 dBm and -15.1 dBm, respectively) with comparable phase noise performance. The simultaneous RP and RF feedback oscillations demonstrated a large increase in carrier power (2.77 dBm) while experiencing an improvement in the far-from-carrier phase noise.

The phase noise measurements were normalized to the oscillator's laser and amplifier power consumption and compared in figure 7 and table 1 (photodetector power consumption was too large and would have diminished the

Table 1: Phase noise comparisons at offset frequencies.

Operation mode	(Normalized power consumption) Phase Noise (dBc/Hz)		
	1kHz Offset	100kHz Offset	1MHz Offset
RP	-53.62	-109.6	-118.4
RF	-53.95	-108.2	-115.8
RP+RF	-54.74	-112.6	**-128.6**

normalization's effectiveness). The RP enhanced RF feedback oscillations had no $1/f^4$ or higher order noise and the close-to-carrier phase noise is dominated by $1/f^3$ flicker noise from both the amplifier and input laser. A 10dB improvement in far-from-carrier phase noise was observed.

CONCLUSION

The 2-coupled-ring resonator based oscillator with a mechanical quality factor of 6,000 and resonant frequency of 175.3 MHz was tested under vacuum (30μTorr) and low temperature (80 K) for different driving schemes. Simultaneous RP and RF feedback induced oscillations resulted in an increased RF output signal power (2.77 dBm) when compared to only RP (-21.4 dBm) and RF feedback (-15.1 dBm) oscillations. The combined driving scheme resulted in more energy stored in the oscillator and a 10dB improvement in far-from-carrier phase noise (1MHz).

REFERENCES
[1] S. Tallur, S. Sridaran and S. A. Bhave, *MEMS 2012*, pp. 19-22.
[2] T. O. Rocheleau, C.T.-C. Nguyen, et al., *MEMS 2013*, pp. 118-121.
[3] S. Sridaran and S. A. Bhave, *Transducers '11*, pp. 2920-23.
[4] T.J. Kippenberg and K. J. Vahala, *Science*, vol. 321, pp. 1172-1176 (2008)
[5] M. Poot, H. Tang, et al, *Phys. Rev. A*, vol. 86, p. 053826 (2012)
[6] A. Schliesser, T. Kippenberg, et al, *Nature Physics*, vol. 4, pp. 415-19 (2008)
[7] G. I. Harris, U. L. Andersen, J. Knittel, W. P. Bowen, *Phys. Rev. A*, vol. 85, p. 061802 (2012)
[8] H. Rokhsari, M. Hossein-Zadeh, A. Hajimiri, K. Vahala, *Appl. Phys. Lett.*, vol. 89, p. 261109 (2006)